The 5G Localization Waveform

Ronald Raulefs, Armin Dammann, Thomas Jost, Michael Walter, and Siwei Zhang

Institute of Communications and Navigation, German Aerospace Center (DLR), Germany
Email: {Ronald.Raulefs, Armin.Dammann, Thomas.Jost, M.Walter, Siwei.Zhang}@DLR.de

***Abstract*—Todays cellular networks have distinct services that come with different requirements, figures of merit, etc. for each application. A communication service such as voice communication relies on latency better than 150 ms and bit error rates lower than 10^{-2}. A vehicular application that controls the brakes of cars in a demanding platoon constellation demands latency in the communication link of less than 1 ms to avoid a crash. Localization is another service which is gaining attention for several years and is mandatory for many applications nowadays. Ubiquitous applications that rely on precise location information are nowadays limited by the best possible accuracy in cellular networks. Only outdoors special GNSS receiver exploiting information gathered from additional measurement units (RTK) allow a degree of precision in the cm-range. For 5G networks we expect to have distinct waveform that achieves a similar accuracy to enable plenty of applications. In the ETSI 22891-100 [1] document different use cases describe a requirement on localization accuracy of less than 1m for a car and of up to 0.1 m for a robot. Nowadays such accuracy cannot by far be reached in the LTE system – even when considering the dedicated positioning reference signals (PRS). Therefore, the PRS pave the way for integrating localization as core feature which deserves an optimized waveform. In addition the new applications (especially with a control loop inside) demand to consider the time to first fix, which describes the latency of the positioning estimation process. Both of these key figures of merit, accuracy and time to first fix, depend on the chosen waveform for localization. Further, the signal structure needs to consider in a dense network the geometrical constellation in 3D of the participating nodes as it influences strongly the performance. The proposed waveform is a multicarrier waveform that jointly enables the access to the localization signal structure simultaneously for multiple nodes in conjunction with the distribution of power on dedicated bands.**

I. Introduction

The history of determining the whereabouts of cellular mobile terminals starts with the first generation of cellular networks. At that time each mobile operated inside one cell, and the location determination was very unprecise [2]. In 1996 the Federal Communications Commission (FCC) demanded that operators fulfill within a limited time frame strict constraints to determine the mobile terminals for 911 emergency calls. In the coming years the effort in the United States focused on meeting the requirements for existing cellular systems. These systems were namely IS-54 and IS-95. In 1999, the standardisation group ETSI and the American T1P1 drafted a document that described the location service for GSM[1] and its successor UMTS[2]. The positioning services in GSM [3] focused on uplink time of arrival (ToA), enhanced observed time difference (E-OTD) and as fall-in solution the cell-ID. In UMTS observed time difference (OTD) with configurable idle times to overcome the cellular interference was introduced together with the cell-ID as fall-in solution (uplink TDoA came later to replace E-OTD). The introduction of E-OTD required reference units, called location measurement units (LMUs), in the network because the base stations were not well enough synchronized. Uplink TDoA (U-TDoA) was easier to realize as calculations were done in the network compared to E-OTD which performed the calculations in the mobile. The FCC was the driving force to supervise strict rules for location accuracy requirements. In 2012 the FCC in Phase II sharpened the demands and requirements by avoiding the simple averaging of multiple measurements. In UMTS and later on in LTE[3], RF pattern matching was added to improve the cell-ID technique [4].

II. Signal Waveforms for Communications and Localisation

Currently different initiatives discuss potential waveforms to cope with the new demands that raise with the 5G cellular communication networks.

In [5] the 5GNOW consortium evaluated different waveforms that focused on different communication demands, such as spectral efficiency for broadband signals, low latency and scalability (100.000 devices with sporadic access).

For future GNSS-based systems the waveform under investigations are also based on multicarrier signal structures [6]. Here the focus of the waveform is on low peak to average power ratio (PAPR) with a multi-node access scheme.

In this paper we put the focus on determining time-based ranging waveform to improve and establish localization as a service with its own waveform.

III. Scenarios

Our key enabler we exploit is a high user/device density and the ability to exploit device-to-device (D2D) links. This enables as we have shown in [7] a dramatic performance improvement of the localization performance. These could be relevant scenarios where location information is important:

- Machine to machine (static and mobile) communication.
- Pedestrians in a mall
- Multiple cars in a GPS-denied environment.

Propagation delay based positioning methods like TDOA require signal reception from 3 base stations (BSs) in order to calculate a 2D mobile terminal (MT) position. Fig. 1 shows an

[1]Global System for Mobile Communications

[2]Universal Mobile Telecommunications System

[3]Long Term Evolution

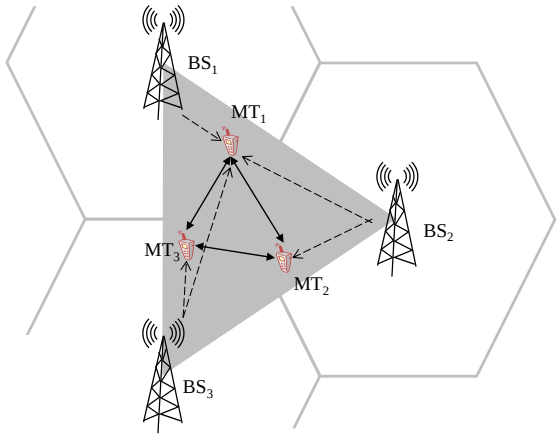

Figure 1. 5G envisages D2D communications, where MTs may cooperate with each other for positioning. If the mesh of D2D links is sufficient, positioning works even if there are less than 3 BSs visible to individual MTs.

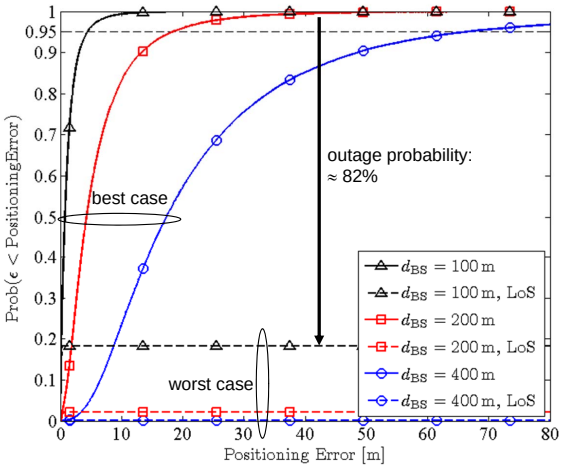

Figure 2. CDF of the MT non-cooperative positioning error for different cell sizes. Results plotted in solid lines assume a zero NLoS bias. Results plotted in dashed lines consider only LoS reception of BS signals.

environment where 3 MTs are located in an area surrounded by 3 BSs. In many environments the probability of receiving signals from 3 different BSs with sufficient quality has shown to be quite low. In the example above only MT_1 receives signals from 3 adjacent BSs indicated by dashed lines in Fig. 1. Therefore, this MT is able to calculate its position using conventional non cooperative mobile radio positioning methods. MT_2 and MT_3 are not connected to a sufficient number of BSs, and therefore, will fail in calculating their positions. With the concept of cooperative positioning a MT additionally observes signals transmitted from other MTs in its neighborhood. If reasonably connected, cooperative positioning is possible even if there are less than 3 BSs visible at each MT, which is intuitively shown in Fig. 1. In our example shown in Fig. 1, the device-to-device (D2D) links between MTs are depicted as bold arrows.

Table I
SYSTEM PARAMETERS.

Parameter		Value
Carrier frequency	f_c	5 GHz
Base station TX power	P_BS	30 dBm
Base station TX signal bandwidth	B_BS	5 MHz, uniform power spectral density
Mobile terminal TX power	P_MT	20 dBm
Mobile terminal TX signal bandwidth	B_MT	1 MHz, uniform power spectral density
Noise power spectral density	N_0	$N_0 = k_\mathrm{B}\,T$
Boltzmann constant	k_B	$1.381 \cdot 10^{-23}\,\mathrm{J/K}$
Noise temperature	T	300 K
Propagation model BS-MT		WINNER C2 Typical Urban (large scale fading)
Propagation model D2D		free space, communication range is limited to r_com
D2D communication range	r_com	50 m
Base station distance	d_BS	100 ... 400 m
Mobile terminal density	D	$\approx 230 \ldots 1850\,\mathrm{km}^{-2}$

A. Non-Cooperative Positioning

In order to show the benefit of cooperative positioning we briefly recall results obtained in [7]. We first start with non-cooperative positioning. It is obvious that for non-cooperative positioning the positioning performance does not depend on the number of MT located in our environment. Thus we uniformly distribute one MT in our area of interest between the BSs and calculate the Cramér-Rao lower bound. We evaluate the statistics in form of cumulative distribution functions (CDFs). For the generation of the CDFs we have used 10000 realizations for the MT position. Fig. 2 shows the results for different BS distances d_BS. The channel model we have used for the BS-MT links distinguishes between line-of-sight (LoS) and non-LoS (NLoS) propagation conditions. The probability of LoS propagation rapidly decreases with increasing dictance between BS and MT. Table I summarizes the system parameters which we have used for our investigations.

As best case we assume that in case of NLoS propagation we do not suffer from an additional bias term (NLoS bias), i.e., we set the NLoS bias to zero. For a inter BS distance of $d_\mathrm{BS} = 400\,\mathrm{m}$ the positioning error is lower than $66.2\,\mathrm{m}$ in $95\,\%$ of the cases. This $95\,\%$ error drops to $4.3\,\mathrm{m}$ for $d_\mathrm{BS} = 100\,\mathrm{m}$.

As worst case we assume that we can detect NLoS propagation and neglect those links. So, we only use links which are in LoS for MT position calculation. In our case this means that if at least one of the links from the MT to the 3 BSs is in NLoS condition, we cannot calculate a position and the MT is in outage. Fig. 2 shows the corresponding results. Already for a BS distance of $d_\mathrm{BS} = 100\,\mathrm{m}$, the MTs are in outage for $82.2\,\%$ of the cases. As the cell size increases, this outage probability rapidly increases to $98\,\%$ and $99.9\,\%$ respectively for the BS distances of $200\,\mathrm{m}$ and $400\,\mathrm{m}$.

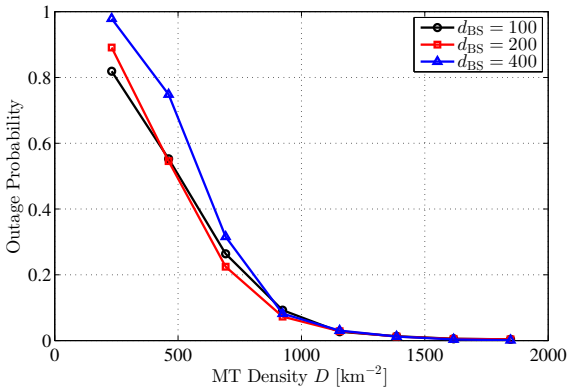

Figure 3. Outage probability P_{out} versus the MT density for different BS distances d_{BS}.

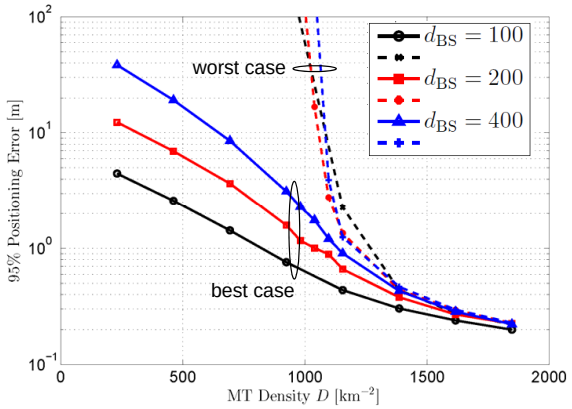

Figure 4. 95 % positioning error versus the MT density for different BS distances d_{BS}.

B. Cooperative Positioning

Now, let us consider cooperative positioning, where additional pseudo range observation from D2D links are available. For the D2D links we assume free space signal propagation. We can expect an increasing probability of NLoS propagation with increasing distance between MTs. Therefore, we limit the communication range to $r_{\mathrm{com}} = 50\,\mathrm{m}$. Within this range we assume LoS propagation.

For an increasing number of MTs, we are interested in both the 95 % positioning error probability and the outage probability if we neglect NLoS links. Figs. 3 and 4 summarize the outage probabilities and 95 % positioning error performances. For the BS-MT links we again distinguish between a best case and a worst case as described in Sec. III-A. For all the considered cell sizes, the outage probability falls below 5 % for a MT density $D > 1100\,\mathrm{MTs/km^2}$ (MTs per square kilometer)[4]. Above that MT density, the 95 % positioning error performance reaches sub-meter accuracy. The 95 % positioning error performance for the worst case converges to that order of magnitude as well.

[4]For comparison note that the mean density of players on a soccer field is approximately $3000\,\mathrm{players/km^2}$.

IV. System Characteristics of Ranging Signals

Key parameters to improve range estimation are signal power and its distribution in the used signal band and the usable bandwidth. The range estimates determine the performance of location by trilateration together with the geometrical constellation. In [7] we could show that the an increase of the density of radio terminals which cooperate with each other overcomes the lack of base stations. Especially in dynamic constellations a dense network improves the performance by sharing the full available bandwidth between multiple terminals concurrently [8]. The concurrent usage of the same bandwidth in dense networks is a strong motivator to apply a multiuser compatible waveform.

V. Localization Waveforms

We propose a waveform that flexibly allocates resources, such as dedicated spectrum and signal power, of the available spectrum so that range estimation could be granted under different service degrees. The usage of coarse geo-information could further help to improve the location estimation by considering the geometrical constellation between the different radio terminals.

Therefore, we propose a localisation waveform with the following combined features:

- flexible bandwidth
- flexible signal power
- flexible subcarrier allocation

A. Triangle Waveform

We consider a parametric waveform which shows triangular shaped power spectrum density (PSD). We can describe the power spectrum density waveform analytically

$$|S(f)|^2 = \begin{cases} (1-\alpha)\,\frac{2}{B} - \frac{4\,(1-2\,\alpha)}{B^2}\,|f|\,, & |f| \le \frac{B}{2} \\ 0, & |f| > \frac{B}{2} \end{cases} \tag{1}$$

as a function of the signal bandwidth B and a 'shaping' parameter $0 \le \alpha \le 1$. Fig. 5(a) shows the corresponding power spectrum densities for different values of α. Note, this waveform description also contains a uniform power spectrum distribution ($\alpha = 0.5$). The corresponding autocorrelation function reads

$$\varphi(\tau) = 2\,\alpha\,\frac{\sin(\pi\,B\,\tau)}{(\pi\,B\,\tau)} + (1-2\,\alpha)\,\frac{\sin^2\left(\pi\,\frac{B}{2}\,\tau\right)}{\left(\pi\,\frac{B}{2}\,\tau\right)^2}, \quad 0 \le \alpha \le 1 \tag{2}$$

and is shown in Fig. 5(b). Parameter α controls the power spectrum density, and therefore, the shape of the autocorrelation function. With an increasing α, the power spectrum at higher frequencies increases. Correspondingly, the steepness of the autocorrelation function increases. This behavior is accounted by the so called squared equivalent signal bandwidth

$$\beta^2 = \frac{\int f^2\,|S(f)|^2\,\mathrm{d}f}{\int |S(f)|^2\,\mathrm{d}f}. \tag{3}$$

For triangular waveforms, the squared equivalent signal bandwidth linearly grows with increasing α as

$$\beta^2 = \frac{B^2}{24}\,(1+2\,\alpha)\,, \qquad 0 \le \alpha \le 1. \tag{4}$$

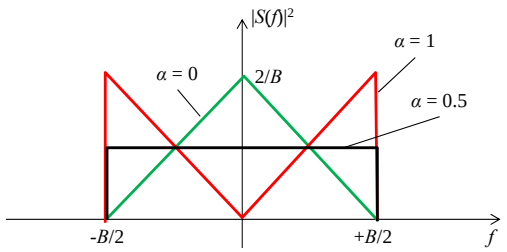

(a) Power spectrum density

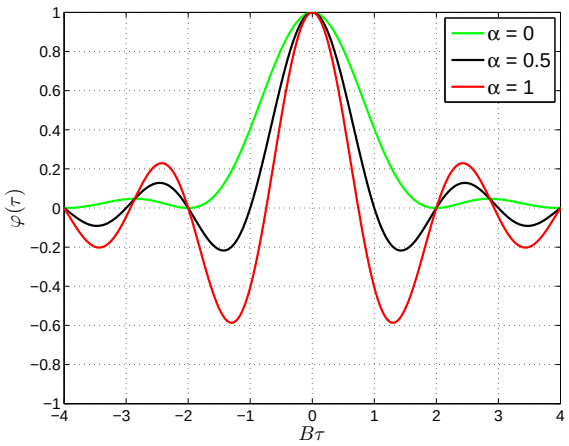

(b) Autocorrelation function

Figure 5. Triangular waveforms

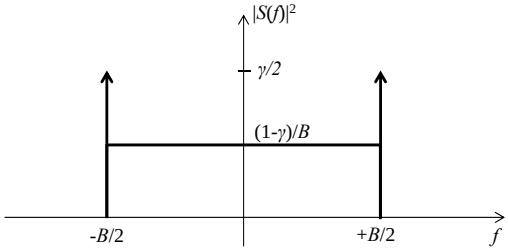

(a) Power spectrum density

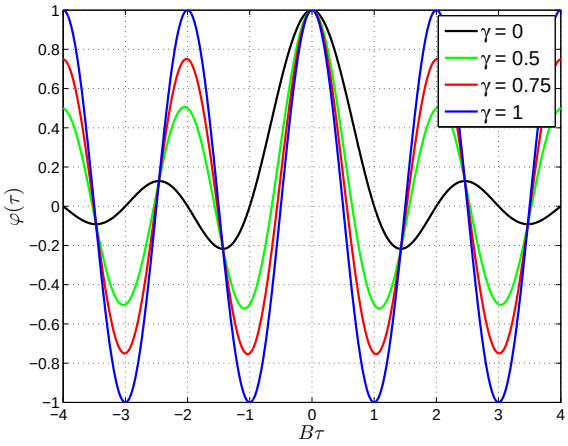

(b) Autocorrelation function

Figure 6. Dirac-rectangular waveforms

B. Dirac Waveform

The considerations above suggest that increased spectral densities at higher frequencies are beneficial for range estimation. In an extreme case we might assign the available signal power to the spectrum edges at $f = \pm\frac{B}{2}$, which results in a dirac-shaped power spectrum density

$$|S(f)|^2 = \frac{1}{2}\left[\delta\left(f+\frac{B}{2}\right)+\delta\left(f-\frac{B}{2}\right)\right] \tag{5}$$

an squared equivalent signal bandwidth of

$$\beta^2 = \frac{B^2}{4}. \tag{6}$$

The corresponding autocorrelation function for this waveform is

$$\varphi(\tau) = \cos(\pi\, B\, \tau)\,. \tag{7}$$

C. Dirac-Rectangular Waveform

As further parametrized waveform we consider a weighted superposition of the Dirac and a rectangular power spectrum density

$$|S(f)|^2 = \begin{cases} \frac{1-\gamma}{B} + \frac{\gamma}{2}\left[\delta\left(f+\frac{B}{2}\right)+\delta\left(f-\frac{B}{2}\right)\right], & |f| \le \frac{B}{2} \\ 0, & |f| > \frac{B}{2} \end{cases} \tag{8}$$

as shown in Fig. 6(a) with autocorrelation function

$$\varphi(\tau) = (1-\gamma)\,\frac{\sin(\pi\, B\, \tau)}{(\pi\, B\, \tau)} + \gamma\,\cos(\pi\, B\, \tau)\,, \tag{9}$$

depicted in Fig. 6(b). The squared equivalent bandwidth is

$$\beta^2 = \frac{B^2}{12}\,(1+2\,\gamma)\,, \qquad 0 \le \gamma \le 1. \tag{10}$$

With $\gamma = 1$ we achieve the Dirac waveform discussed above, and therefore, the maximum possible squared equivalent bandwidth of $\beta^2 = \frac{B^2}{4}$.

D. Dolph-Chebyshev Waveform

The waveforms introduced above have exemplary shown that the steepness of the autocorrelation function's mainlobe increases with increasing equivalent signal bandwidth. However, an improved steepness of the mainlobe comes with increased sidelobe amplitudes, which increases the probability of misleading decisions in an estimator. Dolph-Chebyshev window function [9] provides a parameter to directly control the sidelobe amplitude. It can be defined as the length N discrete Fourier transform of

$$w(k) = \varphi\left(\tau = k\,T_\mathrm{s}\right) = \frac{\cos\left\{N\,\cos^{-1}\left[b\cos\left(\frac{\pi B}{N}\,\tau\right)\right]\right\}}{\cosh\left[N\,\cosh^{-1}(b)\right]} \tag{11}$$

with

$$b = \cosh\left[\frac{1}{N}\,\cosh^{-1}\left(10^{\frac{a}{10}}\right)\right], \tag{12}$$

where $B = \frac{1}{T_\mathrm{s}}$ is the signal bandwidth and T_s the corresponding sampling time. Parameter a denotes the sidelobe attenuation in dB. We consider this function as autocorrelation function $\varphi(\tau)$. Fig. 7(b) shows its graphs for different values of

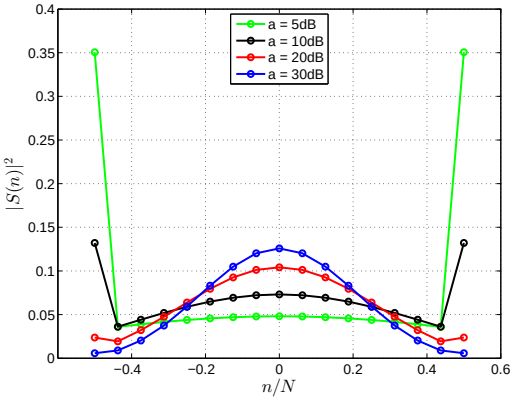

(a) Power spectrum

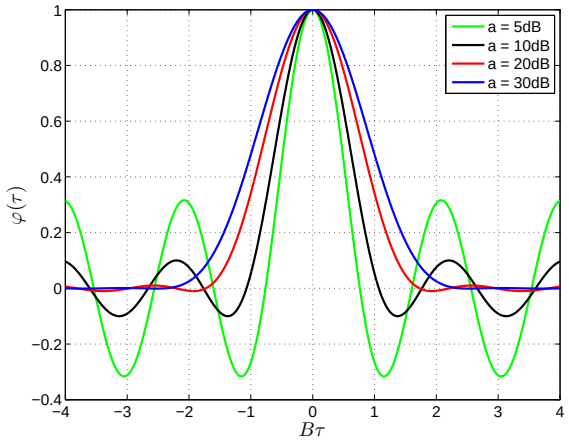

(b) Autocorrelation function

Figure 7. Dolph-Chebyshev waveforms

sidelobe attenuation a and $N = 16$. Note, the autocorrelation function $\varphi(\tau)$ is periodic with period duration $N\,T_\mathrm{s} = \frac{N}{B}$. The power spectrum of the signal is discrete and can be expressed in form of the length N discrete Fourier transform of $w(k)$ as

$$|S(n)|^2 = \frac{1}{N}\sum_{k=0}^{N-1} w(k)\,\mathrm{e}^{-\mathrm{j}\,\frac{2\pi}{N}\,n\,k}, \quad n = -\frac{N}{2},\ldots,+\frac{N}{2}. \tag{13}$$

Fig. 7(a) shows the discrete power spectrum for Dolph-Chebyshev waveforms for different sidelobe attenuations a. Note, as the frequency spacing is $\Delta f = \frac{B}{N}$, the power spectrum shown in Fig. 7(a) covers a frequency range of $-\frac{B}{2},\ldots,+\frac{B}{2}$.

VI. Range Estimation Performance Bounds

The Cramér-Rao lower bound (CRLB) is a lower bound for the achievable variance of any unbiased estimator. For signal propagation delay based range estimation between a transmitter and a receiver, the Cramér-Rao lower bound calculates to

$$\mathrm{CRLB} = \frac{c_0^2}{8\pi^2\,\beta^2\,\mathrm{SNR}}, \tag{14}$$

where c_0 is the speed of light (cf. e.g. [10]). The Cramér-Rao lower bound is inverse proportional to the squared equivalent signal bandwidth β^2 and the signal-to-noise ratio (SNR) at the receiver.

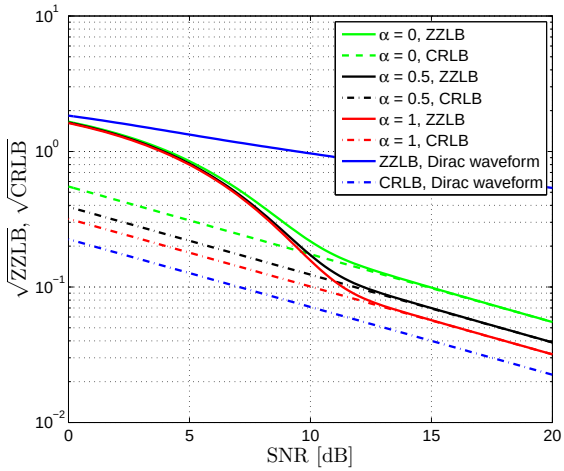

Figure 8. Square root of the ZZLB and CRLB for triangular waveforms.

However, a higher equivalent signal bandwidth comes with the price of higher autocorrelation function sidelobes as shown in Fig. 5(b). In particular at low SNRs an estimator might erroneously decide for such an incorrect sidelobe with non negligible probability. Due to this behavior, the estimator variance rapidly increases for lower SNRs. This threshold effect is not accounted by the Cramér-Rao lower bound, which is known to be tight only for reasonably high SNRs. The Ziv-Zakai lower bound (ZZLB), however, takes this effect into account. We follow results in [11] for this type of bound. Accordingly, the Ziv-Zakai lower bound for range estimation calculates to

$$\mathrm{ZZLB} = c_0^2 \int_0^T \tau\,\left(1-\frac{\tau}{T}\right)\,\phi\left(\sqrt{\mathrm{SNR}\,(1-\varphi(\tau))}\right)\mathrm{d}\tau \tag{15}$$

where

$$\phi(x) = \frac{1}{\sqrt{2\pi}}\int_x^\infty \mathrm{e}^{-t^2/2}\,\mathrm{d}t \tag{16}$$

denotes the Gaussian Q-function. Parameter T describes the length of an observation interval. It is assumed that the signal parameter to be estimated — in our case the signal propagation delay — is equally distributed within $[-T/2\,,\,+T/2]$.

The square root of the CRLB and the ZZLB are shown in Figs. 8-10 in a normalized form, i.e., $T = 10/B$, $B = 1$, $c_0 = 1$. The threshold effect mentioned above is clearly visible for the Ziv-Zakai lower bounds. For increasing SNRs the ZZLBs converge to the corresponding CRLBs. Contrary, the SNR value at which the ZZLB starts to diverge from the CRLB increases with increasing parameter α or, equivalently, with an increasing squared equivalent bandwidth β^2. For the Dirac waveform the ZZLB shows no convergence to the corresponding CRLB. This can be explained by having a look on its autocorrelaton function, which is a cosine. Here, the autocorrelation sidelobe amplitudes are equal to the main lobe

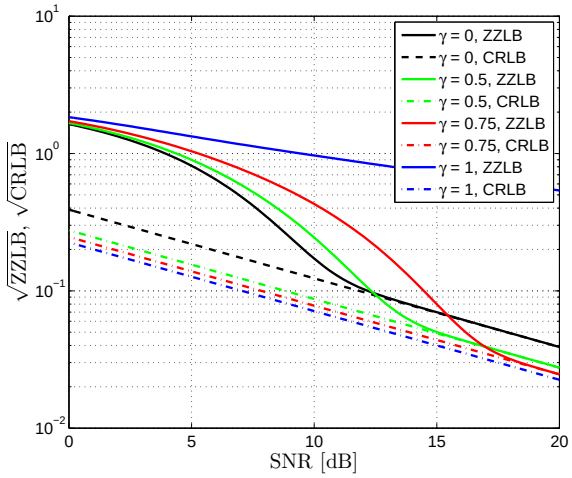

Figure 9. Square root of the ZZLB and CRLB for Dirac-rectangular waveforms.

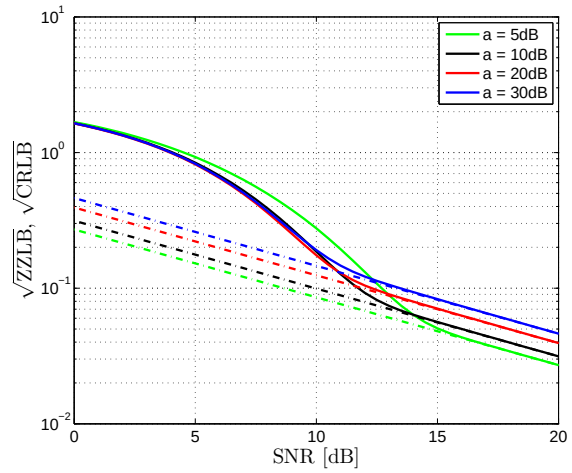

Figure 10. Square root of the ZZLB (solid) and CRLB (dashed) for Dolph-Chebyshev waveforms.

amplitude. In particular decisions for any sidelobe or the main lobe are equiprobable.

The performance results for the triangular wavforms shown in Fig. 8 again indicate that a higher squared equivalent bandwidth is beneficial for range estimation. For this particular waveform $\alpha = 1$ is the preferred choice for all SNRs. This situation changes for the Dirac-rectangular and the Dolph-Chebyshev waveforms shown in Fig. 9 and Fig. 10. Since these waveforms can provide higher equivalent signal bandwidths compared to the triangular waveforms, the performance at high SNRs is increased. However, due to divergence of ZZLB and CRLB at higher SNRs there is an preferable choice for the corresponding waveform parameters γ and a for different SNR regions. In the optimum case for each SNR value there is an optimum choice of these parameters.

The results above indicate that there is a tradeoff between the ranging performances at high and medium to low SNRs. Depending on the available signal power respectively the receiver SNR we might decide for an optimum spectrum form. However, this depends on the local distribution of mobile terminals. Therefore, it is beneficial to keep a 5G positioning waveform flexible with respect to its power spectrum density.

VII. Conclusions and Outlook

In this paper we define the localization service as a unique service that demands different figures of merit compared to many different communication services. Applications and as well communication services itself exploit location information for optimal performance in future networks. The dedicated waveform we propose increases the flexible use of spectrum dedicated for range estimation. The flexible use of spectrum and signal power is important to exploit the high node density of devices to achieve high localization performance. The flexible use allows a parallel access to the same spectrum by distinctly separating the different range signals. The concurrent access is needed in dynamic scenarios to optimally determine the location and exploit the most favorable geometrical constellation.

Acknowledgment

This work was partially supported by the EU project HIGHTS (High precision positioning for cooperative ITS applications) MG-3.5a-2014-636537 and the DLR project Dependable Navigation.

References

[1] ETSI, "Study on new services and markets technology enablers," ETSI, http://www.3gpp.org/DynaReport/22891.htm, Tech. Rep. 1.0, November 2015.

[2] M. Hatay and T. Nagatsu, "Mobile location using signal strength measurements in a cellular system," *Vehicular Technology, IEEE Transactions on*, vol. 29, no. 2, pp. 245–252, May 1980.

[3] "Overview of 2G LCS technnologies and standards," in *3GPP TSG SA2 LCS Workshop*, London, UK, Jan. 2001, source: Motorola Inc. [Online]. Available: ftp://ftp.3gpp.org/workshop/Archive/0101LCS/Docs/PDF/LCS-010019.pdf

[4] 3GPP TS 25.305, *Universal Mobile Telecommunications System (UMTS); Stage 2 functional specification of User Equipment (UE) positioning in UTRAN (3GPP TS 25.305 version 11.0.0 Release 11)*, 3rd Generation Partnership Project Std., 09 2012.

[5] G. Wunder, M. Kasparick, T. Wild, F. Schaich, Y. Chen, M. Dryjanski, M. Buczkowski, S. Pietrzyk, N. Michailow, M. Matthe, I. Gaspar, L. Mendes, A. Festag, G. Fettweis, J.-B. Dore, N. Cassiau, D. Ktenas, V. Berg, B. Eged, and P. Vago, "5GNOW: Intermediate frame structure and transceiver concepts," in *Globecom Workshops (GC Wkshps), 2014*, Dec 2014, pp. 565–570.

[6] M. Vergara, F. Antreich, M. Meurer, and G. Seco-Granados, "Spreading code design for a MC-CDMA based GNSS pilot signal," ser. Proceedings of the 5th ESA Workshop on Satellite Navigation User Equipment Technologies (NAVITEC). ESA, December 2010.

[7] A. Dammann, R. Raulefs, and S. Zhang, "On prospects of positioning in 5G," in *Proceedings IEEE ICC 2015 - Workshop on 5G & Beyond - Enabling Technologies and Applications*, London, UK, Jun. 2015.

[8] R. Raulefs, S. Zhang, and C. Mensing, "Bound-based spectrum allocation for cooperative positioning," *Transactions on Emerging Telecommunications Technologies*, Jan. 2013.

[9] F. Harris, "On the use of windows for harmonic analysis with the discrete Fourier transform," *Proceedings of the IEEE*, vol. 66, no. 1, pp. 51–83, Jan 1978.

[10] S. M. Kay, *Fundamentals of Statistical Signal Processing — Estimation Theory*. Prentice Hall, 1993.

[11] C. Musso and J.-P. Ovarlez, "Improvement of the Ziv-Zakai lower bound for time delay estimation," in *15th European Signal Processing Conference (EUSIPCO 2007)*, Poznan, Poland, Sep. 2007, pp. 960–964.